applied sciences

MDPI

Article

A Mechatronics-Embedded Pneumatic Soft Modular Robot Powered via Single Air Tube

Yu Zhang [1], Yubin Liu [1,*], Xin Sui [1], Tianjiao Zheng [1], Dongyang Bie [2], Yulin Wang [1], Jie Zhao [1] and Yanhe Zhu [1,*]

1 State Key Laboratory of Robotics and System, Harbin Institute of Technology (HIT), Harbin 150001, China; yuzhang_hit@163.com (Y.Z.); suixinhit@163.com (X.S.); hitzhengtianjiao@163.com (T.Z.); wangyulinhit@163.com (Y.W.); jzhao@hit.edu.cn (J.Z.)

2 The Institute of Robotics and Automatic Information Systems, College of Computer and Control Engineering, and the Tianjin Key Laboratory of Intelligent Robotics, Nankai University, Tianjin 300071, China; bdy@nankai.edu.cn

* Correspondence: liuyubin@hit.edu.cn (Y.L.); yhzhu@hit.edu.cn (Y.Z.)

Received: 22 April 2019; Accepted: 30 May 2019; Published: 31 May 2019

check for updates

Abstract: Soft modular robots have advantages, including infinite degrees of freedom and various configurations. Most soft robots are actuated by inflating air pressure into their chambers. However, each chamber is connected to a tube that provides the air supply, which incurs drag and intertwining problems that influence the robot's motion. Moreover, the number of chambers directly affects the deformations and motion capabilities of the robot. Therefore, the crucial issue is the structure of a soft modular robot that can share an air source without reducing the number of chambers and can guarantee the deformations of the robot. In this paper, a novel mechatronics-embedded soft module was designed and manufactured, which has an air supply sharing function. Therefore, the soft modular robot can be powered via a single air tube. In addition, a wireless platform to control the air pressure of the module was built, and an experimental model was established to obtain the relationship between the deformation and pressure of the module. Four experiments were performed under different conditions. The experiments' results indicate the bending capability of the module. Moreover, hooking object, twisting motion, and bionic gesture experiments demonstrate the validity of the module's air pressure sharing function. Therefore, the air sharing supply approach proposed in this paper can be used as a reference to solve the tube drag problem of soft modular robots.

Keywords: soft modular robot; mechatronics-embedded soft module; air pressure sharing; bionic motion

1. Introduction

The concept of modular robots has been proposed since the 1980s to solve the universal property and flexibility problems of robots with fixed configurations [1]. A modular robot consists of unified modules with the same structure and function to realize reconfigurable configurations for adapting to various tasks and changeable environments. The unified module has communication, controller, actuator, sensor and connecting mechanisms, which can connect with each other to form different configurations. Many researchers have developed rigid modular robots, including Molecubes [2], Yamor [3], Polybot [4], ATRON [5], CONRO [6], M-TRAN [7], SuperBot [8], UBot [9,10], and Seremo [11]. These modular robots can alter their structure by connecting the different faces of their modules. However, rigid modular robots have finite degrees of freedom, and rigid materials are dangerous for fragile objects and operating personnel. Therefore, the use of soft materials to replace rigid materials to manufacture modular robots is a novel research direction.

Soft modular robots have advantages including infinite degrees of freedom and various configurations [12]. Soft modules are manufactured using soft materials, such as silica gel or rubber, which have characteristics of flexibility and continuous deformation. Therefore, many researchers have studied soft modular robots, including omnidirectional soft robots [13], rotary soft module and bending soft module [14], three types of pneumatically actuated soft modules (SoBL) [15], the soft modular robot with connecting part [16], elastomeric hollow cubes with magnetic connecting mechanisms [17], bidirectional bending modules [18], pneumatic actuators with four chambers [19], multi-spherical modular soft robots [20–23], bending-type fluidic elastomer actuators [24], modular soft robots with voice coil actuators [25], soft-bodied caterpillar-like modular robots [26], and vacuum-powered soft pneumatic actuator (V-SPA) modules [27,28].

Some researchers have concentrated their attention on the structure of the soft module. Kurumaya presented the rotary soft module and bending soft module, which can be combined with other actuators as part of a complete manipulator system [14]. Lee designed three types of pneumatically actuated soft modules, which can connect with each other through a unified connecting part [15]. Zhang manufactured and presented a pneumatic soft modular robot with a novel connecting mechanism to achieve a docking function [16]. Luo designed a chamber's structure of soft module, which has a bidirectional bending ability [24].

Meanwhile, a number of researchers have concentrated on the soft modular robot's bionic motion. Jun proposed a reconfigurable omnidirectional soft robot based on the locomotion of caterpillars. The pneumatic soft robot is capable of moving with three DOFs (degree of freedoms) on a plane [13]. Vergara proposed a new soft modular robot to simulate replicating morphogenetic movements of an embryo, which provide tangible models of cell behavior [17]. Hamill manufactured a soft module with four chambers and analyzed the gait of a soft hexapod robot [19]. Fei presented a multi-sphere modular robot to realize an obstacle avoidance motion [21]. Umedachi proposed a soft-bodied caterpillar-like modular robot to simulate caterpillar motion [25].

Nevertheless, most soft modular robots are actuated by inflating air pressure. Therefore, each chamber of the soft module needs to be connected with an air tube, which provides air pressure to actuate the deformation of the module. However, air tubes incur drag and intertwining problems that affect the motions of the soft modular robots. Moreover, the problems cannot be solved by reducing the number of chambers, which directly affects the deforming ability of the soft robot.

Therefore, it is critical to design the soft modular robot with a shared air source and guarantee the deformations. A few researchers have investigated the gas source sharing issue. Gunjan Agarwal proposed a vacuum-powered soft pneumatic actuator (V-SPA), which shared a vacuum power supply [27,28]. However, the V-SPA has a novel solenoid valve, manufactured by piezoelectric ceramic technology, which is a non-universal technology for researchers to manufacture soft modular robots. Therefore, we present a mechatronics-embedded pneumatic soft modular robot (MeSMR) powered via single air tube. The MeSMR provides a common and convenient approach to design and manufacture of soft modular robot.

There are five sections in this paper. Section 2 introduces the design and manufacture process of the soft module. Control systems and experimental modelling are presented in Section 3. Section 4 illustrates experiments and results of the MeSMR.

2. Design and Manufacture of Soft Module

2.1. Structure and Manufacture of Soft Module

Soft modular robots mostly utilize solenoid valves that open or close to provide air-flow. Therefore, soft modular robots need air tubes connected to chambers. Moreover, air tubes easily twine around each other, which greatly affect the movement of soft robots. However, solenoid valves are too large to be placed into a soft module. To solve the problem of excessive tubes, a novel structure for the soft module is designed in this section.

Figure 1 shows the manufacture process of the soft module, which includes a gas controller, silica gel module and gas supply connection. The gas controller (Part A) consists of a seal cover, a wireless control board system, a battery and three gas flow valves. The gas flow valve is composed of a motor base, a reduction motor, an external thread connection, an internal thread sleeve and a silica gel plug. The reduction motor is controlled by the control board, which drives the external thread to facilitate the silica gel plug's linear motion along the motor base. Three fan-shaped chambers are blocked by the silica gel plugs when the motor is unpowered. When the control board receives a wireless signal, the output shaft of the reduction motor connects to the screw and enables the linear motion of the silica gel plug. Then, the air pressure inflates the fan-shaped chamber to realize deformation.

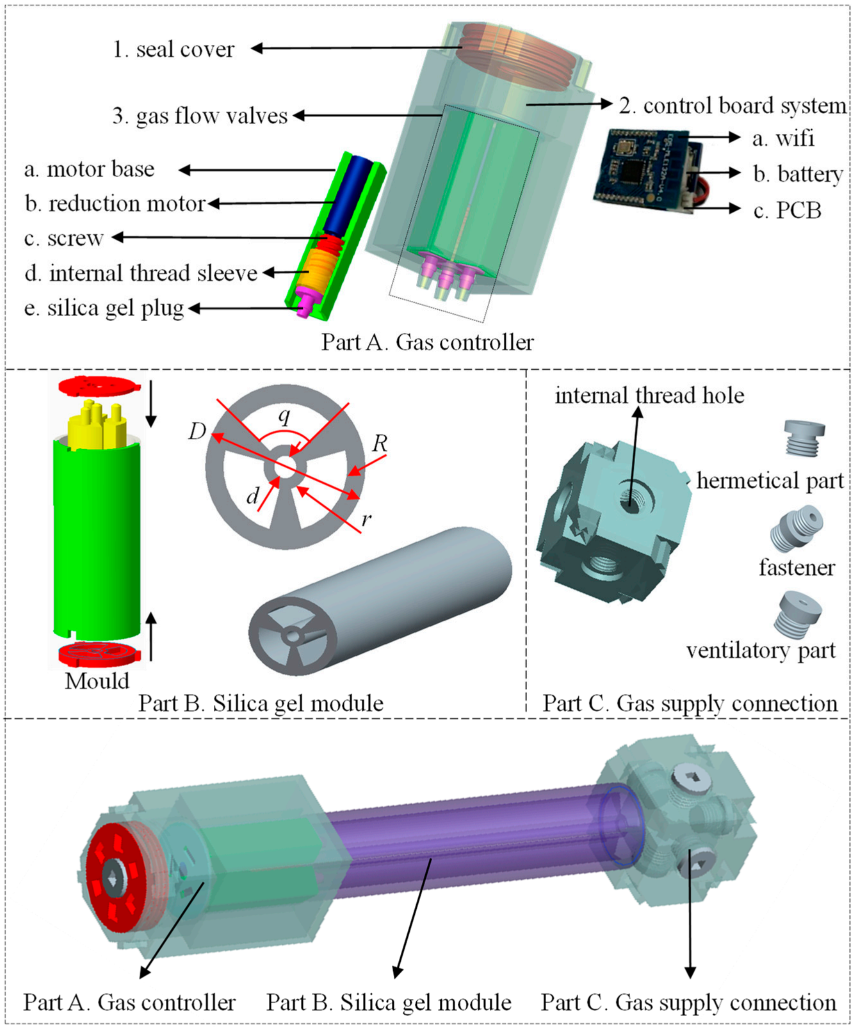

Figure 1. Manufacture process for the soft module.

The silica gel module (Part B) has four chambers. Three fan-shaped chambers are used to render the module's deformation, and one cylindrical chamber is used to transport air pressure for the fan-shaped chambers. The cylindrical chamber's diameter is denoted as d, which is on the center of the module. The angle between any two connecting lines of the fan-shaped chambers' center points is 120°. Other design parameters of the module are listed as follows: The diameter D, the angle between the two sides of the sector q, the arcs of the sector R and r. The module is made by silica gel demolding technology.

The gas supply connection (Part C) has one internal thread hole in each face, which is used to connect with the threaded parts. The threaded parts have three types of structure: Hermetical, fastener, and ventilated parts. The hermetical part is used to seal the internal thread hole. The fastener is used to connect with two gas supply connections. One end of the ventilated part connects with the internal thread hole, and the other end of the ventilated part is used to connect with the air tube. The gas supply connection has six connecting faces. One of the connecting faces is used to fix the silica gel module, and the other connecting faces are used to connect with the other modules or air tube.

The gas controller and gas supply connection are bonded on the two ends of the silica gel module by utilizing Smooth-On silicone rubber adhesive. The molds and gas supply connection are manufactured by 3-D printing technology. Therefore, the modules are connected by the gas supply connection and threaded parts, which can form various configurations and have air pressure sharing functions.

2.2. Parameter Optimization of the Soft Module

To design a soft module with satisfactory performance, the relationship between the structure parameters and the deformation of the module is a key factor. Therefore, the material characteristics are obtained by uniaxial tensile tests with a 1 cm square length silica gel slice. The stress and strain are obtained and shown in Table 1. Then, the uniaxial tensile results and Workbench software's Yeoh model are used to fit the deformation curve. Therefore, the parameters of deformation energy $C_1 = 0.036$ MPa and $C_2 = 0.007$ MPa are obtained, and the fitting curves are shown in Figure 2.

Table 1. The results of uniaxial tensile tests with a silica gel slice.

Stress(MPa)	0.040	0.055	0.073	0.101	0.127	0.141	0.163	0.206	0.233	0.253
Strain(mm)	0.078	0.294	0.509	0.734	0.968	1.082	1.207	1.431	1.676	1.874

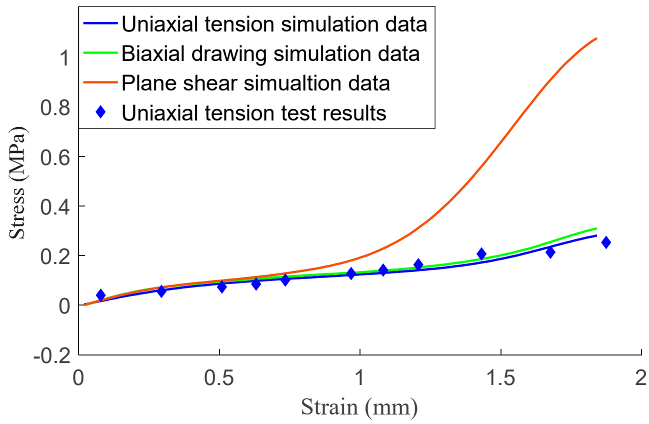

Figure 2. The fitting curves by the Yeoh model.

The parameters of the soft module $D = 22$ mm, $L = 95$ mm, and $q = 90°$ are defined. The other parameters of the module are obtained by contrasting the deformations with various conditions. Figures 3–5 illustrate the module's bending angles with different parameters. Figure 3 shows an increase in the bending angles with radius R of the fan-shaped chamber. Moreover, the increasing rate of the bending angle of the module at $R = 8.5$ mm is higher than that of the other parameters. The increasing rate of the module with the radius r of the fan-shaped chamber are shown in Figure 4. However, the diameter d of the cylindrical chamber is limited to the radius r. Figure 5 shows that the effect of the diameter d on the bending angle of the module is small. Moreover, the thickness of the module is too slim when the diameter d is too large and the radius r is too small to manufacture. Therefore, the following parameters are chosen: $R = 8.5$ mm, $r = 3$ mm and $d = 3$ mm.

To prove the rationality of the parameter selection, we used the Abaqus software to simulate the bending states of the module with optimized parameters. Figure 6 shows an increase in the bending angles of the module with air pressure, and the bending angle is 180° when the air pressure 50 kPa. Therefore, the soft module has an appropriate bending ability with the designed structure.

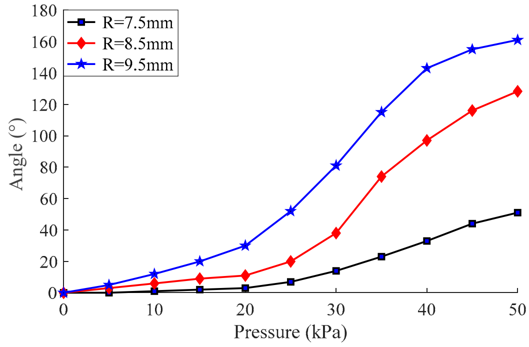

Figure 3. Bending angles of the soft model with the radius *R*.

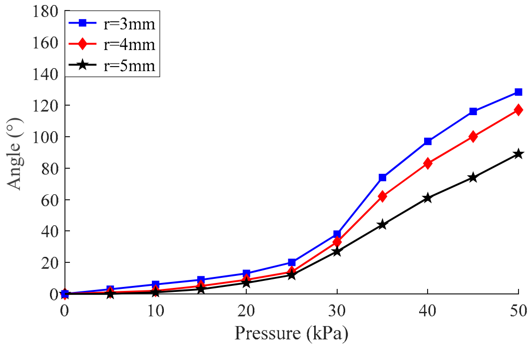

Figure 4. Bending angles of the soft model with the radius *r*.

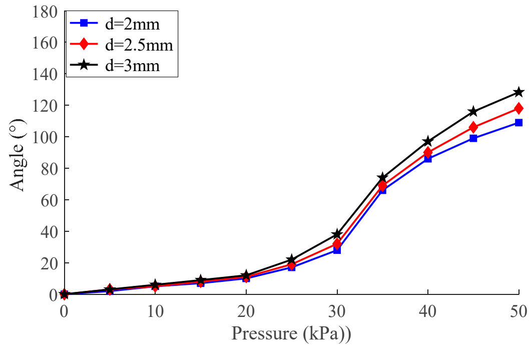

Figure 5. Bending angles of the soft model with the diameter *d*.

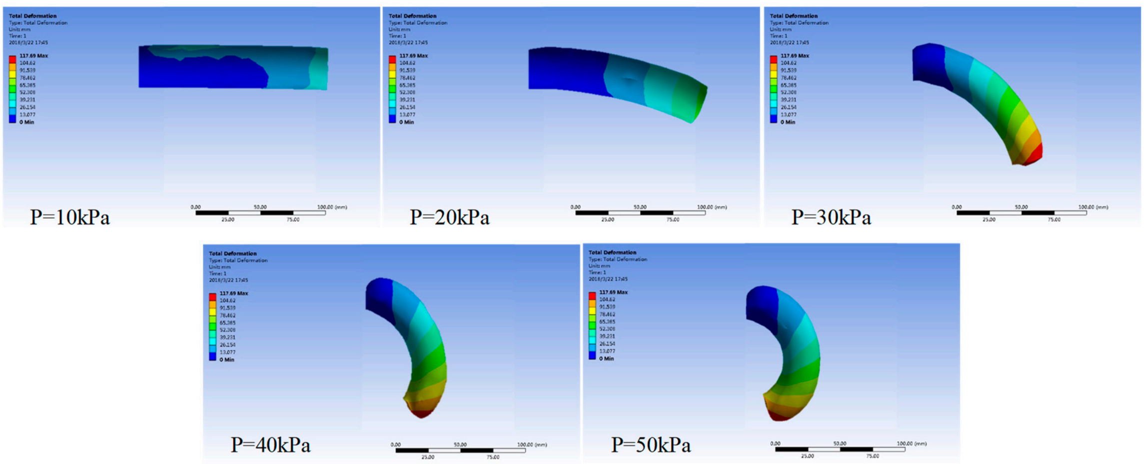

Figure 6. The bending states of the module by Abaqus software simulation.

3. Control System and Experimental Model

3.1. Control System for the MeSMR

The soft modules are actuated by the inflating air pressure. Therefore, air pressure is a very important parameter to influence the deformation of the module. In order to obtain the relationship between pressure and deformation of the soft module, a closed loop control system is established using a pressure sensor. The experiment platform has an inflating/deflating function, as shown in Figure 7. The dash frame is the control system for the MeSMR, which includes DC power, PCB, Wi-Fi module, air pump, solenoid valves, and controller.

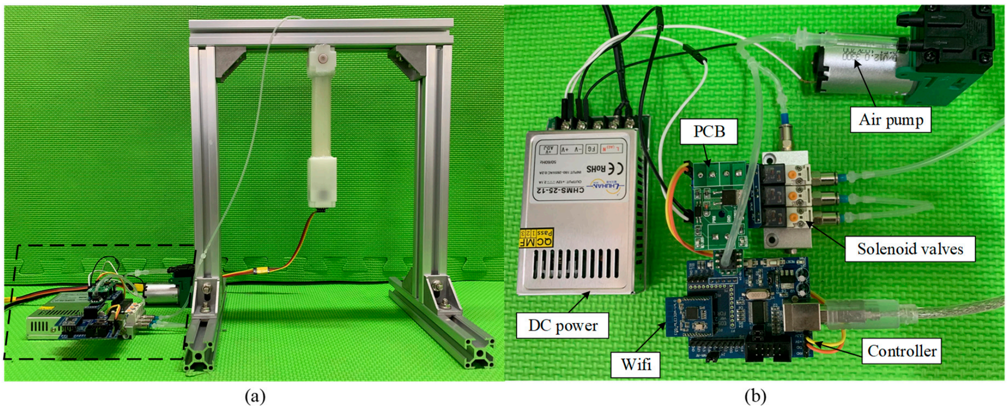

Figure 7. The Experiment platform: (**a**) Experiment platform; (**b**) control system for the MeSMR.

The control system has a quick-speed inflating function and a slow-speed inflating function. The quick-speed inflating function is used when the pressure is far below the desired value (greater than 5 kPa). The slow-speed function is used for precise control when the pressure of the module is close to the desired value (smaller than 5 kPa).

Therefore, the control principle of a platform based on proportional–integral–derivative (PID) theory is

$$\Delta u(k) = k_p \times (e(k) - e(k-1)) + k_i \times e(k) + k_d \times (e(k) - 2 \times e(k-1) + e(k-2)) \quad (1)$$

where $\Delta u(k)$ is the output increment of the controller on the k^{th} sampling period; $e(k)$ is the pressure error on the k^{th} sampling period; and k_p, k_i and k_d are the proportion coefficient, integral constant, and differential constant of the PID controller, respectively.

The controller's parameters are $k_p = 50$, $k_i = 10$, and $k_d = 0$ when working in a quick-speed state. The parameters of the slow-speed state are $k_p = 100$, $k_i = 20$, and $k_d = 0$. Figure 8 shows the curves of the input pressure and actual pressure of the PID controller. The maximum error of the stable pressure is 0.9029 kPa, which illustrates the validity of the controller.

The soft module showed a well repeatable performance as shown in Figure 9. In these experiments, the soft module was inflated from 0 kPa to 60 kPa, and then deflated to 0 kPa. The results, which are shown in the same color, are obtained in a one-time experiment. Meanwhile, the experiments were repeated three times with the same conditions. The hysteretic characteristic is also presented in Figure 9. The bending angles in the process of decreasing pressure are larger than those in the process of increasing pressure, which is caused by properties of the silica gel. Meanwhile, the largest hysteretic angle is 5.5 degrees.

Figure 10 illustrates the 2D workspace of the soft module, which is the longitudinal section of its 3D workspace, forming an area enclosed by two curves. The edges of the 3D workspace of the soft module are two surfaces shown in Figure 11. The maximum displacement in the radial direction is 24 mm, and the farthest and nearest points in the axial direction are 190 mm and 229 mm, respectively.

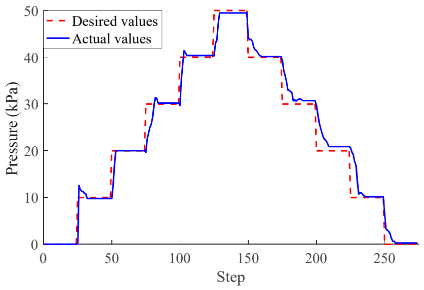

Figure 8. Comparison of the desired and actual values of the control system.

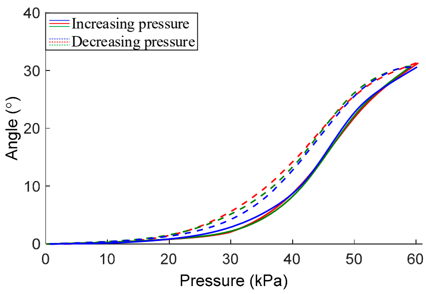

Figure 9. The hysteretic characteristic of the soft module.

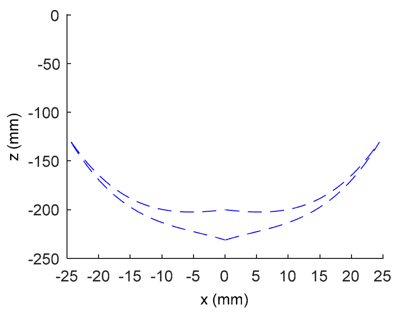

Figure 10. 2D workspace of the soft module.

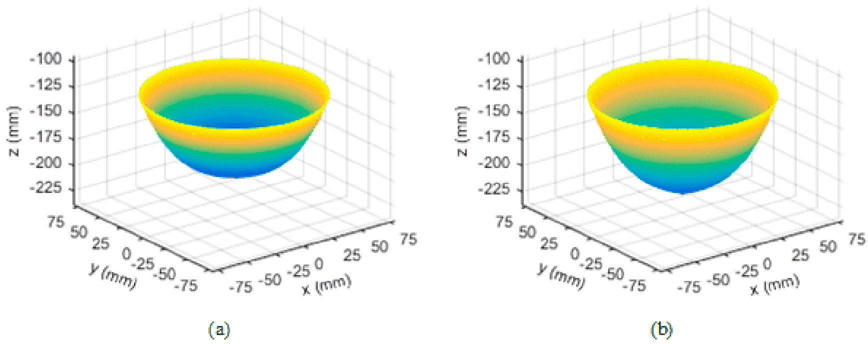

Figure 11. 3D workspace of the soft module: (**a**) The nearest surface of workspace; (**b**) the farthest surface of workspace.

3.2. Experimental Model between Deformation and Pressure of the Module

The response characterizations of the soft module are influenced by the chamber's structure and material's properties. Thus, the experimental relationship model was established based on experimental values. As shown in Figure 12, the fixed coordinate system O-xyz is built on point O, which is the center point on one end of the module. Meanwhile, the posture sensor (JY61-MPU6050, Telesky, Shenzhen, China) is fixed on the other end of the module to measure the bending angle. The chambers are numbered Chamber 1, Chamber 2 and Chamber 3 respectively.

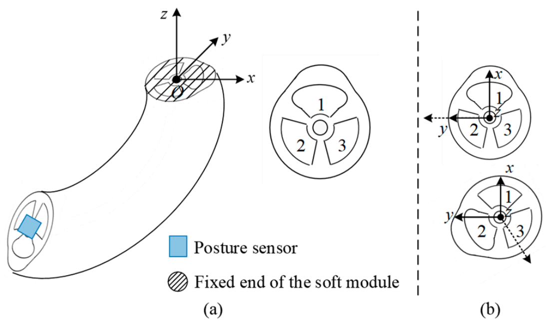

Figure 12. Coordinate system and deformation analysis of the soft module: (**a**) Coordinate system; (**b**) deformation analysis.

The experiments were repeated three times with the same module parameters, and the experimental model are shown in Figure 13. The points with different shapes and colors represent the experimental values, which were obtained by inflating air pressure into Chamber 1. The module's bending states vary with the pressure every 10 kPa (from 0 kPa to 60 kPa). The dash lines are the fitting curves of the experimental values. The solid line is the experimental model, which is the average values of three fitting curves. The results showed that the bending angle increases with pressure and the curvature of curves is a substantial increase when pressure values were over 30 kPa. Figure 14 shows the comparison results between the simulation and experimental model. The trend of the experimental results was basically in accord with the trend of simulation values. Moreover, the maximum error of the results between the simulation and experiments was less than 9 degrees.

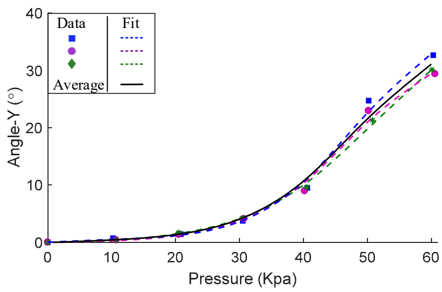

Figure 13. The experimental model of chamber 1.

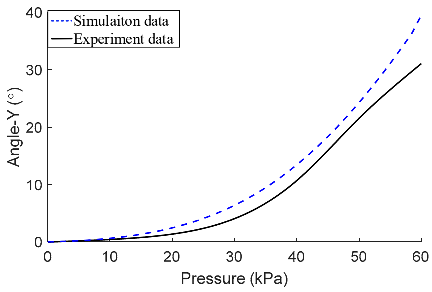

Figure 14. The comparison results between the simulation and experimental model of Chamber 1.

The bending angles of the module by inflating air pressure into Chamber 2 are shown in Figure 15. The module bending states vary with the pressure every 10 kPa (from 0 kPa to 60 kPa). The points with the same shape represent experimental values under different pressures. The experiments were repeated three times with the same conditions. As shown in Figure 15, the dash lines are the fitting curves of the experimental values; the solid line represents the experimental model, which is the average values of the fitting curves. The results were three-dimensional curves because the rotate axis was not coincident to the axis of the fixed coordinate system. Chambers 2 and 3 are axial symmetry about x-axis. Thus, the bending angle of Chamber 3 can be obtained by the experimental model of Chamber 2. Figure 16 illustrates the comparison of the simulation and experimental model. The maximum error of the results between the simulation and experiment is less than 10 degrees.

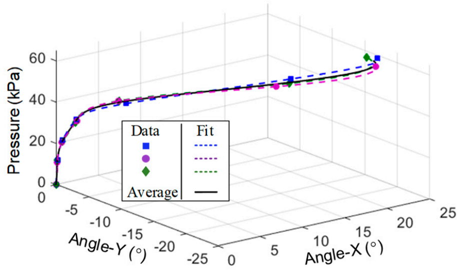

Figure 15. The experimental model of chamber 2.

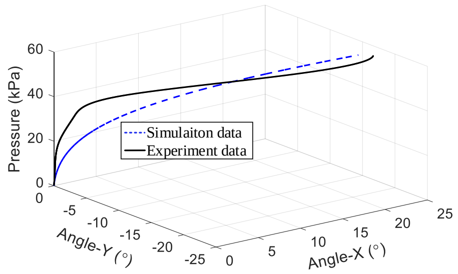

Figure 16. The comparison results between the simulation and experimental model of Chamber 2.

As shown in Figures 14 and 16, there were some deviations of the simulations and experimental results because of the idealization errors. Particularly, the main factor incurring the deviation is the thickness uniformity of the soft module, which cannot be entirely consistent with that in the simulation.

4. Experiments and Results

4.1. Bending Motion

Figure 17 presents the module in which air is pumped at a pressure ranging from 0 kPa to 40 kPa, into two chambers to realize 3-D motion. Figure 18 shows the flow chart of controlling process for the soft model. The results illustrate the effectiveness of the control system and the reliability of the gas supply connecting part, which can supply air pressure to all chambers of the soft module using only one air tube.

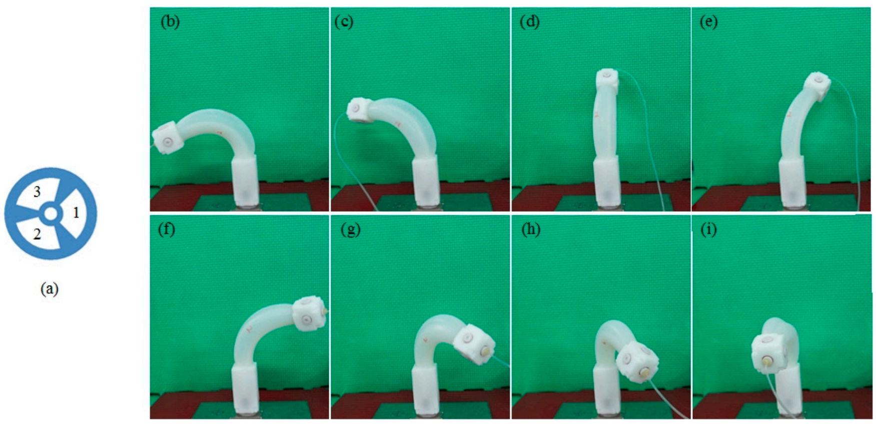

Figure 17. Three-dimensional motion of the module: (**a**) Cross section of module; (**b**–**i**) a series of frames captured from video for three-dimensional motion.

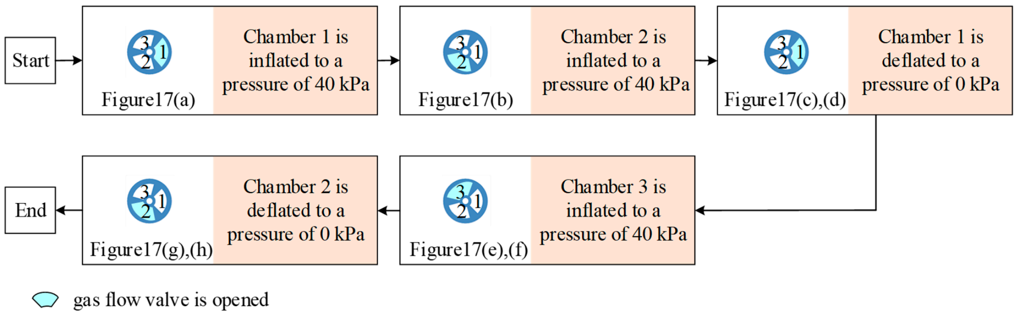

Figure 18. The flow chart of three-dimensional motion.

4.2. Hooking Object

The soft robot consists of Module A and Module B, as shown in Figure 19. The chambers of the module are numbered Y*i* (*i* = 1, 2, 3), where Y is the number of modules and *i* is the number of modules Y's chamber. Therefore, A1, A2 and A3 are expressed in three chambers of Module A, as shown in Figure 19.

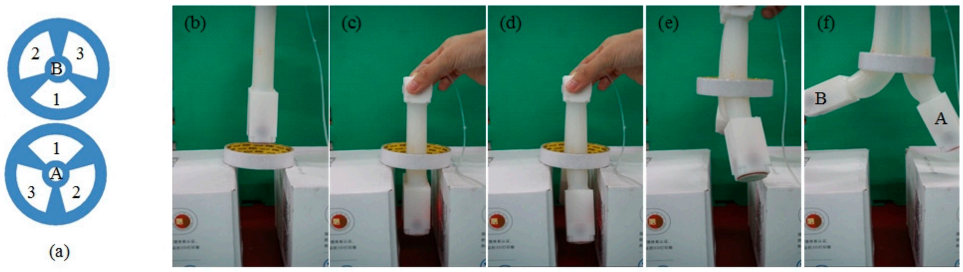

Figure 19. Hooking object of the soft robot: (**a**) Cross section of hooking configuration robot; (**b**–**f**) a series of frames captured from video for hooking object.

Figure 19 also shows the process of hooking a hollow object using a soft robot. The robot is inflated with air to form an anchor-like shape until 30 kPa. Accordingly, the robot can pick up a hollow object. Moreover, the sharing air pressure function of the gas controller part of the module is verified. In future work, we will develop a carrying capacity for the module to realize robots picking up heavy objects.

4.3. Twisting Motion

The crossing configuration robot consists of four modules, and the identifiers of modules and chambers are shown in Figure 20, which also illustrates that the robot has a grasping ability and can twist the object. The robot is actuated, i.e., all modules' Chamber 1 are inflated with air until 40 kPa, to form the shape of a claw for holding the object, as shown in Figure 20c,d. Then, the air is pumped into Chamber 2 of each module to produce a torsional force. Therefore, the object can be twisted by the crossing configuration robot, as shown in Figure 20e.

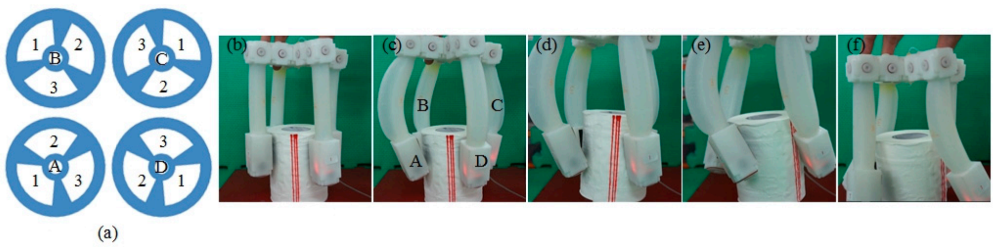

Figure 20. Twisting motion of the soft robot: (**a**) Cross section of the crossing configuration robot; (**b**–**f**) a series of frames captured from video for twisting motion.

As the experimental result shows, four modules share air pressure with one air supply and accomplish a twisting motion. Therefore, the problem of too many tubes, which incurs drag and pull, is effectively solved.

4.4. Bionic gesture

As shown in Figure 21, the soft robot is composed of five soft modules, and each module is similar to the finger of the human hand. The robot can form three types of gestures, namely, OK, Yeah, and Love. The pressure values of the different gestures are shown in Table 2.

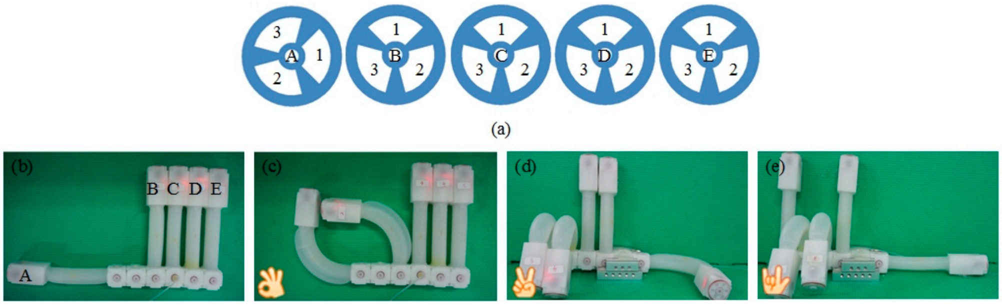

Figure 21. Bionic gestures of the soft robot: (**a**) cross section of fingers; (**b**) initial state of fingers; (**c**) OK gesture; (**d**) Yeah gesture; (**e**) Love gesture.

Table 2. Pressure values of the different gestures.

Gesture	Chambers/Values (kPa)			
OK	A1/45	B3/45	B1/30	——
Yeah	A1/40	A3/40	D1/45	E1/45
Love	C1/45	D1/45	——	——

In Table 2 and Figure 20, the soft robot forms the OK gesture when the pressure values of A1, B1, and B3 are 45 kPa, 30 kPa and 45 kPa, respectively. When the figure forms the Yeah gesture, the values are 40 kPa for A1 and A3 and 45 kPa for D1 and E1. The Love gesture can also be formed by inflating the air pressure of C1 and D1 to 45 kPa. Therefore, the soft robot can form various gestures by inflating different values of air pressure into the modules' chambers. Moreover, the gas controller can supply air for five modules at the same time. This method provides an effective approach for researchers to design soft modular robots.

5. Conclusions

In this paper, we designed a mechatronics-embedded pneumatic soft module with a novel structure and introduced the manufacturing process. The soft module is made from silica gel, which has a continuous deformation characteristic. Moreover, the hysteretic characteristic and 3D workspace of the soft module are analyzed. In order to obtain the relationship between the deformation and pressure of the module, the experimental models are established and compared with simulations. Furthermore, we perform four types of experiments of the MeSMR, including bending motion, hooking object, twisting motion and bionic gesture, on a wireless control platform. The results illustrate the reliability of the mechatronics-embedded module and the effectiveness of the air pressure sharing function.

The MeSMR proposed in this paper can realize air sharing functions via a signal air tube, which effectively solves the dragging and intertwine problems of excessive air tubes, although the MeSMR has the limitation of parallel inflation and deflation of the actuators. The achieved results can provide the references for researchers to design soft modular robots in the future. Based on the current experimental results, we will continue to research the motions of the MeSMR with different configurations. Such work will enhance the adaptability of soft modular robots to various tasks.

Author Contributions: Conceptualization, Y.Z. (Yu Zhang), Y.Z. (Yanhe Zhu) and J.Z.; methodology, Y.Z. (Yu Zhang), Y.L. and T.Z.; validation, Y.Z. (Yu zhang), Y.L. and X.S.; data curation, X.S., D.B. and Y.W.; writing—original draft preparation, Y.Z. (Yu Zhang); all authors have read and approved the final manuscript.

Funding: This work was supported in part by the Joint Research Fund (U1713201) between the National Natural Science Foundation of China (NSFC) and Shen Zhen and in part by the NSFC under Grant 61673137.

Conflicts of Interest: The authors declare no conflict of interest.

References

1. Yim, M.; Shen, W.-M.; Salemi, B.; Rus, D.; Moll, M.; Lipson, H.; Klavins, E.; Chirikjian, G.S. Modular self-reconfigurable robot systems—Challenges and opportunities for the future. *IEEE Robot. Autom. Mag.* **2007**, *14*, 43–52. [CrossRef]
2. Zykov, V.; Chan, A.; Lipson, H. Molecubes: An Open-Source Modular Robotics Kit. In Proceedings of the IROS-2007 Workshop on Self-Reconfigurable Robots and Systems and Application, San Diego, CA, USA, 2 November 2007; pp. 3–6.
3. Moeckel, R.; Jaquier, C.; Drapel, K.; Dittrich, E.; Upegui, A.; Jan Ijspeert, A. Exploring adaptive locomotion with YaMoR, a novel autonomous modular robot with Bluetooth interface. *Ind. Robot Int. J.* **2006**, *33*, 285–290. [CrossRef]
4. Yim, M.; Duff, D.G.; Roufas, K.D. PolyBot: A modular reconfigurable robot. Robotics and Automation. In Proceedings of the IEEE International Conference on Robotics and Automation (ICRA), San Francisco, CA, USA, 24–28 April 2000; pp. 514–520.
5. Jorgensen, M.W.; Ostergaard, E.H.; Lund, H.H. Modular ATRON: Modules for a Self-Reconfigurable Robot. In Proceedings of the IEEE/RSJ International Conference on Intelligent Robots and Systems (IROS), Sendai, Japan, 28 Stemperber–2 October 2004; pp. 2068–2073.
6. Castano, A.; Shen, W.M.; Will, P. CONRO: Towards deployable robots with inter-Robots metamorphic capabilities. *Auton. Robot* **2000**, *8*, 309–324. [CrossRef]
7. Kurokawa, H.; Tomita, K.; Kamimura, A.; Kokaji, S.; Hasuo, T.; Murata, S. Distributed self-reconfiguration of M-TRAN III modular robotic system. *Int. J. Robot. Res.* **2008**, *27*, 373–385. [CrossRef]
8. Shen, W.M.; Krivokon, M.; Chiu, H.; Everist, J.; Rubenstein, M.; Venkatesh, J. Multimode lcomotion via SuperBot reconfigurable robots. *Auton. Robots* **2006**, *20*, 165–177. [CrossRef]
9. Zhao, J.; Wang, X.; Jin, H.; Bie, D.; Zhu, Y. Automatic locomotion generation for a UBot modular tobot—Towards both high-speed and multiple patterns. *Int. J. Adv. Robot. Syst.* **2015**, *12*, 1–10. [CrossRef]
10. Wang, X.; Jin, H.; Zhu, Y.; Chen, B.; Bie, D.; Zhang, Y.; Zhao, J. Serpenoid polygonal rolling for chain-type modular robots: A study of modeling, pattern switching and application. *Robot. Comput. Integr. Manuf.* **2016**, *39*, 56–67. [CrossRef]
11. Bie, D.; Gutiérrez-Naranjo, M.A.; Zhao, J.; Zhu, Y. An approach to the bio-inspired control of self-Reconfigurable robots. In Proceedings of the 12th International Conference on Bio-Inspired Computing: Theories an Application (BIC-TA), Harbin, China, 1–3 December 2017; pp. 24–38.
12. Lipson, H. Challenges and opportunities for design, simulation, and fabrication of Soft robots. *Soft Robot.* **2014**, *1*, 21–27. [CrossRef]
13. Zou, J.; Lin, Y.; Ji, C.; Yang, H. A Reconfigurable Omnidirectional Soft Robot Based on Caterpillar Locomotion. *Soft Robot.* **2018**, *5*, 164–174. [CrossRef]
14. Kurumaya, S.; Phillips, B.T.; Becker, K.P.; Rosen, M.H.; Gruber, D.F.; Galloway, K.C.; Suzumori, K.; Wood, R.J. Modular Soft Robotic Wrist for Underwater Manipulation. *Soft Robot.* **2018**, *5*, 399–409. [CrossRef]
15. Lee, J.Y.; Kim, W.B.; Choi, W.Y.; Cho, K.J. Soft robotic blocks: Introducing SoBL, a fast-build modularized design block. *IEEE Robot. Automat. Mag.* **2016**, *23*, 30–41. [CrossRef]
16. Zhang, Y.; Zheng, T.; Fan, J.; Li, G.; Zhu, Y.; Zhao, J. Nonlinear modeling and docking tests of a soft modular Robot. *IEEE Access* **2019**, *7*, 11328–11337. [CrossRef]
17. Vergara, A.; Lau, Y.S.; Mendoza-Garcia, R.F.; Zagal, J.C. Soft modular robotic cubes: Toward replicating morphogenetic movements of the embryo. *PLoS ONE* **2017**, *12*, 1–17. [CrossRef] [PubMed]

18. Luo, M.; Skorina, E.H.; Tao, W.; Chen, F.; Ozel, S.; Sun, Y.; Onal, C.D. Toward modular soft robotics: Proprioceptive curvature sensing and sliding-mode control of soft bidirectional bending modules. *Soft Robot.* **2017**, *4*, 117–125. [CrossRef]
19. Hamill, S.; Peele, B.; Ferenz, P.; Westwater, M.; Shepherd, R.F.; Kress-Gazit, H. Gait synthesis for modular soft robots. In Proceedings of the International Symposium on Experimental Robotics (ISER), Tokyo, Japan, 3–6 October 2016; pp. 669–678.
20. Pang, W.; Fei, Y.; He, W. Study on motion process of modular soft robot. In Proceedings of the International Conference on Machine Learning and Cybernetics, Jeju Island, Korea, 10–13 July 2016; pp. 146–151.
21. Fei, Y.; Gao, H. Nonlinear dynamic modeling on multi-spherical modular soft robots. *Nonlinear Dyn.* **2014**, *78*, 831–838. [CrossRef]
22. Fei, Y.; Wang, X. Study on nonlinear obstacle avoidance on modular soft robots. *Nonlinear Dyn.* **2015**, *82*, 91–898. [CrossRef]
23. Fei, Y.; Pang, W. Analysis on nonlinear turning motion of multi-spherical soft robots. *Nonlinear Dyn.* **2017**, *88*, 883–892. [CrossRef]
24. Luo, M.; Agheli, M.; Onal, C.D. Theoretical modeling and experimental analysis of a pressure-operated soft robotic snake. *Soft Robot.* **2014**, *1*, 136–145. [CrossRef]
25. Nemitz, M.P.; Mihaylov, P.; Barraclough, T.W.; Ross, D.; Stokes, A.A. Using voice coils to actuate modular soft robots: Wormbot, an Example. *Soft Robot.* **2016**, *3*, 198–204. [CrossRef]
26. Umedachi, T.; Trimmer, B.A. Autonomous decentralized control for soft-bodied caterpillar-like modular robot exploiting large and continuum deformation. In Proceedings of the IEEE/RSJ International Conference on Intelligent Robots and Systems (IROS), Daejeon, South Korea, 9–14 October 2016; pp. 292–297.
27. Agarwal, G.; Robertson, M.A.; Sonar, H.; Paik, J. Design and computational modeling of modular, compliant robot assembly for human lumbar unit and spinal cord. *Sci. Rep.* **2017**, *7*, 1–11. [CrossRef]
28. Robertson, M.A.; Paik, J. New soft robots really suck: Vacuum powered systems empower diverse capabilities. *Sci. Robot.* **2017**, *2*, 1–27. [CrossRef]